

# Electronic Inhomogeneity and Vortex Disorder in Superconducting $\text{Sr}_{0.75}\text{K}_{0.25}\text{Fe}_2\text{As}_2$

Can-Li Song,<sup>1</sup> Yi Yin,<sup>1,2</sup> Martin Zech,<sup>1</sup> Tess Williams,<sup>1</sup> Michael Yee,<sup>1</sup> Gen-Fu Chen,<sup>3</sup> Jian-Lin Luo,<sup>3</sup> Nan-Lin Wang,<sup>3</sup> Eric W. Hudson,<sup>4</sup> and Jennifer E Hoffman<sup>1,\*</sup>

<sup>1</sup>*Department of Physics, Harvard University, Cambridge, MA 02138, USA*

<sup>2</sup>*Physics Department, Zhejiang University, Hangzhou, 310027, China*

<sup>3</sup>*Beijing National Laboratory for Condensed Matter Physics and Institute of Physics, Chinese Academy of Sciences, Beijing 100190, China*

<sup>4</sup>*Department of Physics, The Pennsylvania State University, University Park, PA 16802, USA*

(Dated: December 14, 2012)

We use scanning tunneling microscopy to investigate the surface structure, superconducting and vortex properties in the hole-doped superconductor  $\text{Sr}_{0.75}\text{K}_{0.25}\text{Fe}_2\text{As}_2$  ( $T_c=32$  K). We resolve the long debate over the nature of the  $\text{AFe}_2\text{As}_2$  cleaved surface, finding a dominant Sr/K termination with  $1 \times 2$  reconstruction and ubiquitous superconducting gap, with rarer patches of gapless, unreconstructed As termination. The superconducting gap varies by  $\sigma/\bar{\Delta}=16\%$  on a  $\sim 3$  nm length scale, with average  $2\bar{\Delta}/k_B T_c=3.6$  in the weak coupling limit. At 9 T we observe isotropic vortices which provide a measure of the superconducting coherence length  $\xi = 2.8$  nm, and constrain the pairing symmetry. Furthermore, we observe a vitreous vortex phase and quantify its correlation length in comparison to other iron-based superconductors. The comparison leads us to suggest the importance of dopant size mismatch as a cause of dopant clustering and a new avenue to optimize vortex pinning for increased critical current.

PACS numbers: 68.37.Ef, 74.55.+v, 74.70.Xa, 74.25.Uv

The recent discovery of high transition temperature ( $T_c$ ) iron-based superconductors (Fe-SCs) [1] has provoked much excitement in condensed matter physics, and launched a new era in the search for the key to high- $T_c$  superconductivity [2]. Like cuprates, Fe-SCs exhibit a layered structure with electronically active superconducting planes separated by buffer layers, and the superconductivity develops from antiferromagnetic parent compounds upon chemical doping. In addition to enabling superconductivity, the dopants are potential sources of nanoscale phase separation [3], and crystalline [4] and electronic disorder [5–7], which may in turn lead to  $T_c$  suppression [8] and vortex pinning [9]. With the diversity of possible dopants in Fe-SCs, it has remained an elusive challenge to characterize and categorize their nanoscale effects.

The scanning tunneling microscope (STM) is an ideal tool to study the nanoscale properties of correlated electron materials. STM studies of Fe-SCs have presented several controversial results [10]. First, the cleaved  $\text{AFe}_2\text{As}_2(001)$  surface showed both  $1 \times 2$  and  $\sqrt{2} \times \sqrt{2}$  reconstructions with unclear origin: either a  $1/2$ -layer of A or a reconstruction of a complete As layer. Second, spectroscopic images of optimally electron-doped  $\text{Ba}(\text{Fe}_{1-x}\text{Co}_x)_2\text{As}_2$  cleaved at  $\sim 25$  K revealed nanoscale variations in the superconducting gap  $\Delta$  on a length scale of several nanometers [5]. However, studies of the same compound cleaved at room temperature found a shorter  $\Delta$  correlation length of  $\sim 0.8$ - $1.0$  nm, closely matching the average Co separation for a random dopant distribution ( $\sim 1.0$  nm), which prompted the hypothesis that gap variations may be caused by the disorder of individual Co atoms [7]. Finally, the  $1 \times 2$  surface of

electron-doped  $\text{BaFe}_{1.8}\text{Co}_{0.2}\text{As}_2$  displayed a disordered vortex lattice without observed vortex core Andreev bound states [5]. In contrast, the domain-like surface of hole-doped  $\text{Ba}_{0.6}\text{K}_{0.4}\text{Fe}_2\text{As}_2$  displayed a hexagonal vortex lattice with pronounced vortex core bound states [11]. It has been proposed but not verified that the vortex discrepancy may be explained by stronger scattering from the in-plane Co dopants than the out-of-plane K dopants.

To address these controversies,  $\text{Sr}_{1-x}\text{K}_x\text{Fe}_2\text{As}_2$  is a unique system with specific advantages. Gao *et al* predicted no surface reconstruction in the As-terminated  $\text{SrFe}_2\text{As}_2$  surface [12] (in contrast to As-terminated  $\text{BaFe}_2\text{As}_2$ ). This makes it easy to distinguish between a complete As layer and a partial Sr layer. Moreover, gap and vortex mapping in this material can test the hypothesis that individual strong-scattering Co dopants are responsible for the gap inhomogeneity and vortex pinning differences between  $\text{BaFe}_{1.8}\text{Co}_{0.2}\text{As}_2$  and  $\text{Ba}_{0.6}\text{K}_{0.4}\text{Fe}_2\text{As}_2$ .

Here we utilize a home-built cryogenic STM to systematically study the hole-doped superconductor  $\text{Sr}_{0.75}\text{K}_{0.25}\text{Fe}_2\text{As}_2$  (underdoped,  $T_c=32$  K). The single crystal samples were prepared by a FeAs flux method detailed elsewhere [13]. We cleave the samples in situ at  $\sim 25$  K and insert them immediately into the STM for imaging at 6 K. To obtain a tunneling current, we apply a bias to the sample while the tip is held at virtual ground. All spectra were measured using a lock-in technique with a 1.0 mV rms bias modulation at 1110 Hz. Figure 1(a) shows the schematic crystal structure of  $\text{Sr}_{1-x}\text{K}_x\text{Fe}_2\text{As}_2$ . Due to the strong covalent bond between Fe and As ions, the cleavage likely occurs in the Sr/K plane, leaving  $\sim 1/2$  Sr/K on either exposed

side to balance the chemical valence. Figure 1(b) typifies the most commonly observed surface with local  $1 \times 2$  stripes [14, 15]. Occasionally for low- $T$  cleaves, the metastable As-terminated  $1 \times 1$  surface may be expected [12]. Previous STM imaging of  $\text{SrFe}_2\text{As}_2$  samples cleaved at 77 K showed no such  $1 \times 1$  patches [14], and instead both  $1 \times 2$  and  $\sqrt{2} \times \sqrt{2}$  orderings in the entire cleaved surface were explained as the bare but reconstructed As layer; whereas a previous study of  $\text{Sr}_{1-x}\text{K}_x\text{Fe}_2\text{As}_2$  cleaved at 10 K showed only a very small  $1 \times 1$  patch with no accompanying spectroscopy [15]. However, we observe larger  $1 \times 1$  patches [Fig. 1(c)], constituting  $\sim 5\%$  of the surface, with average As-As atomic spacing of approximately 0.4 nm. This first observation of large areas of  $1 \times 1$  ordering provides the final unambiguous proof that the dominant  $1 \times 2$  and  $\sqrt{2} \times \sqrt{2}$  observed structures arise from a  $1/2$ -Sr/K layer. The bright rows in our  $1 \times 1$  regions are identified as residual Sr/K atoms. We then record differential  $dI/dV$  spectra on both Sr/K- and As-terminated surfaces, illustrated in Figs. 1(d) and 1(e), respectively. In stark contrast to the universal superconducting gap with clear coherence peaks on the Sr/K-terminated surface, no symmetric superconducting gap is observed on the As-terminated surface, which is probably caused by the strong polarity of the latter surface. The cleaved structure therefore plays a crucial role in superconductivity at the surface, in some cases preventing even proximity-induced superconductivity from appearing.

To further explore the effect of cleaved surface structure on superconductivity, we survey  $dI/dV$  spectra at all locations within the cyan box in Fig. 1(b). These spectra can be analyzed to yield maps of  $\Delta(\vec{r})$ , zero bias conductance (ZBC)  $Z(\vec{r})$ , and coherence peak strength  $C(\vec{r})$ , as displayed in Figs. 2(a)-2(c). All three maps show spatial inhomogeneity. The average  $\bar{\Delta} = 5.0$  meV with a standard deviation of  $\sigma = 0.8$  meV gives a fractional variation  $\sigma/\bar{\Delta} = 16\%$ , larger than the 12% variation found in  $\text{BaFe}_{1.8}\text{Co}_{0.2}\text{As}_2$  [5]. The small reduced gap  $2\bar{\Delta}/k_B T_c \sim 3.6$  suggests weak coupling in  $\text{Sr}_{0.75}\text{K}_{0.25}\text{Fe}_2\text{As}_2$ .

In order to investigate the spectral shape, all spectra are binned based on  $\Delta$ , with their averages plotted in Fig. 2(d). Evidently, the spectra with smaller  $\Delta$  tend to show larger ZBC and stronger coherence peaks. To quantify this trend, we compute the cross-correlation between  $\Delta(\vec{r})$  and  $Z(\vec{r})$  as well as coherence peak strength  $C(\vec{r})$  [Fig. 2(e)]. Together with the autocorrelation of the gap map, we note that the characteristic length scale for all correlations is  $\sim 3$  nm, exceeding the average separation ( $\sim 0.8$  nm) between individual K dopants. We therefore suggest that the K dopants exhibit nanoscale phase separation [16], clustering to form K-rich and K-poor regions. This can more effectively relax the strain caused by the large ion size mismatch between  $\text{K}^+$  (146 pm) and  $\text{Sr}^{2+}$  (126 pm) [17]. Due to the

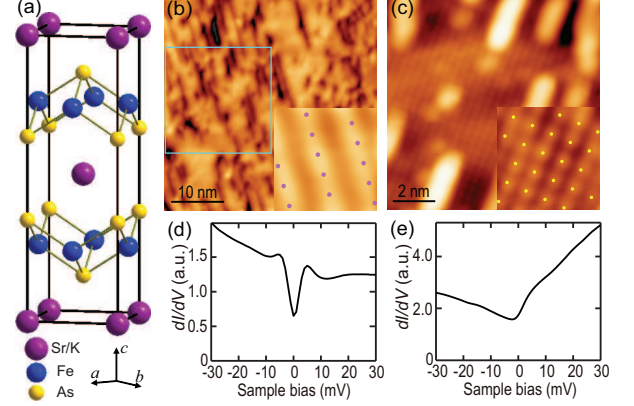


FIG. 1. (color online) (a) Schematic crystal structure of  $\text{Sr}_{1-x}\text{K}_x\text{Fe}_2\text{As}_2$ . (b) STM topography ( $V_s = -100$  mV,  $I = 35$  pA) of the commonly observed  $\text{Sr}_{0.75}\text{K}_{0.25}\text{Fe}_2\text{As}_2$  surface with  $1 \times 2$  stripe order. Inset shows a zoom-in of the stripe with the magenta dots denoting Sr/K atoms ( $V_s = -100$  mV,  $I = 30$  pA,  $2 \text{ nm} \times 2 \text{ nm}$ ). (c) STM topography ( $V_s = -100$  mV,  $I = 350$  pA) showing As-terminated  $1 \times 1$  surface, decorated by sparse Sr/K rows. Inset shows magnification of the  $1 \times 1$  surface with the yellow dots denoting As atoms ( $V_s = -100$  mV,  $I = 350$  pA,  $2 \text{ nm} \times 2 \text{ nm}$ ). (d, e) Spatially averaged  $dI/dV$  spectra in (b) and (c) regions, respectively. Tunneling gap was stabilized at  $V_s = -100$  mV and  $I = 300$  pA.

high sensitivity of superconductivity on the chemical doping [18], the resultant K clusters could account well for our observed electronic inhomogeneity. Meanwhile, the apparent anticorrelation between  $\Delta(\vec{r})$  and  $C(\vec{r})$  may stem from the presence of the competing SDW gap [14, 18, 19]. In regions of smaller K-doping, the local SDW gap would be relatively enhanced, which would suppress  $Z(\vec{r})$  and reduce the low energy states available to contribute to  $C(\vec{r})$ , and furthermore cause these reduced superconducting coherence peaks to appear as shoulders shifted outwards on the larger-SDW-gapped background, enhancing  $\Delta(\vec{r})$ .

Magnetic vortices are technologically important, as the superconducting critical current  $J_c$  is limited by the vortex pinning strength. Vortices are also scientifically valuable for determining the superconducting coherence length  $\xi$  [5, 11] and pairing symmetry [20], and serving as windows into competing phases [21]. Figure 3(a) shows the vortices in a 9 T  $c$ -axis magnetic field as a map of  $dI/dV$  at the filled state coherence peak ( $-5$  meV). The vortices locally suppress the superconducting coherence peaks, and appear as purple-black features with depressed conductance. To better emphasize the vortices, Voronoi cells are overlaid onto the image. From the Voronoi cell size, we estimate the average flux per vortex  $\Phi = 2.1 \pm 0.1 \times 10^{-15}$  Wb, which is consistent with one magnetic flux quantum,  $\Phi_0 = 2.07 \times 10^{-15}$  Wb.

In sharp contrast to the hexagonal vortex lattice

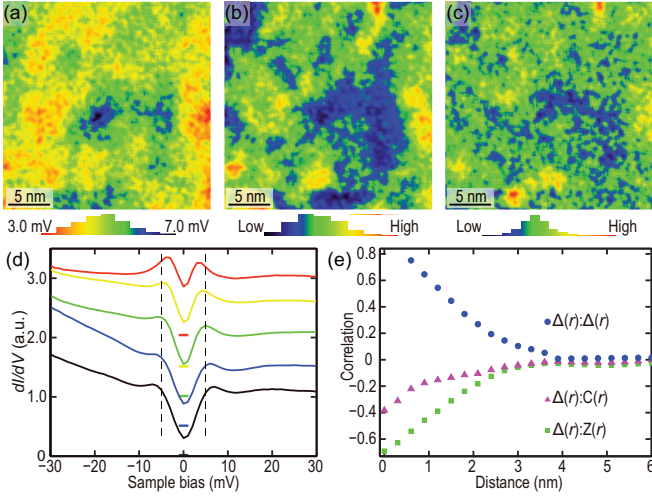


FIG. 2. (color online) (a-c) Maps of  $\Delta(\vec{r})$  (half the distance between coherence peaks),  $Z(\vec{r})$ , and  $C(\vec{r})$  (average conductance at the two peaks). (d) Binned and averaged spectra for five ranges of gap  $\Delta$  ( $\Delta_{\min}$ -3.8, 3.8-4.7, 4.7-5.5, 5.5-6.3, 6.3- $\Delta_{\max}$  meV from top to bottom), color-coded to match those in (a). The spectra have been vertically offset for clarity, with their zero-conductance positions marked by correspondingly colored horizontal lines. Vertical dashes at  $\pm 5$  meV are guides to the eye. (e) Azimuthally averaged autocorrelation of  $\Delta(\vec{r})$ , and cross-correlations of  $\Delta(\vec{r})$  with  $Z(\vec{r})$  and  $C(\vec{r})$ . Raw spectra are used in (d), but spectra were normalized by their backgrounds to compute  $Z(\vec{r})$  and  $C(\vec{r})$  in (b) and (c). Backgrounds were extracted from a cubic fit to the conductance for  $|V| > 10$  mV. The normalization procedure does not affect the signs of the correlations in (e).

which indicates negligible pinning in  $\text{Ba}_{0.6}\text{K}_{0.4}\text{Fe}_2\text{As}_2$  [11], the vortices in  $\text{Sr}_{0.75}\text{K}_{0.25}\text{Fe}_2\text{As}_2$  do not form an ordered lattice. Instead, similar to electron-doped  $\text{Ba}(\text{Fe}_{1-x}\text{Co}_x)_2\text{As}_2$  [5, 22], short-range hexagonal order (vortex glass phase) is justified based on the following two tests. First, the relative distances  $d_{ij} = |r_i - r_j|$  are calculated for all vortex pairs at positions  $r_i$  and  $r_j$ . Figure 3(b) plots the histogram of the observed  $d_{ij}$ . The pronounced peak at the smallest distance of  $\sim 16.4$  nm coincides almost exactly with the expected lattice constant  $a = \sqrt{2\Phi_0/\sqrt{3}H}$  ( $\sim 16.3$  nm, the first vertical line) for a perfect hexagonal vortex arrangement at 9 T. However, with increasing distance the experimental histogram peaks cease to match the corresponding hexagonal lattice separations. This presents the first indication that the vortices are of short-range hexagonal order. Second, Fig. 3(c) shows the Delaunay triangulation by connecting all nearest neighbor vortex sites. Each vortex, surrounded by a closed Voronoi polygon, is color coded in terms of the coordination number. The statistics of the coordination number and angles of Delaunay triangles are plotted in Figs. 3(d) and 3(e), respectively. Two-thirds of vortices are six-fold coordinated, and more importantly, the

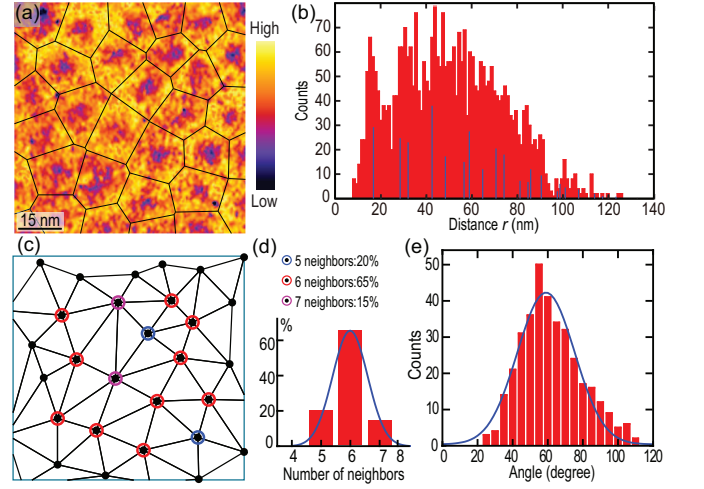


FIG. 3. (color online) A  $80 \text{ nm} \times 80 \text{ nm}$   $dI/dV$  map at  $V_s = -5$  meV, recorded in a 9 T magnetic field. The vortex centers are determined by 2D Gaussian fitting. (b) Histograms of the vortex pair distances  $d_{ij}$  from (a) and another similar  $100 \text{ nm} \times 100 \text{ nm}$  vortex map. Vertical blue lines correspond to the positions and relative weight of pair distances for an ideal hexagonal vortex lattice at 9 T. (c) Delaunay triangulation (black lines) of the vortex lattice in (a). Each vortex is color-coded based on the number of its nearest neighbors. (d, e) Coordination number and Delaunay angle distributions on the border-free regions. Solid blue lines are the Gaussian fits.

Delaunay angle distribution shows a single pronounced peak at  $\sim 60^\circ$ . All this evidence consistently supports a short-range hexagonal order of the vortex arrangement, indicative of strong vortex pinning in  $\text{Sr}_{0.75}\text{K}_{0.25}\text{Fe}_2\text{As}_2$ .

To gain insight into the internal vortex structure, we register all vortex centers, then average the density of states around 48 vortices, as depicted in Fig. 4(a). In contrast to the two- and four-fold symmetric vortices in FeSe [20] and LiFeAs [23], the vortices in  $\text{Sr}_{0.75}\text{K}_{0.25}\text{Fe}_2\text{As}_2$  are nearly isotropic. This observation does not support the claims of  $d$ -wave pairing in more overdoped  $\text{A}_{1-x}\text{K}_x\text{Fe}_2\text{As}_2$  materials [24], although it leaves open the possibility that the isotropy stems from thermal smearing [23] or impurity scattering [25]. Figure 4(b) shows a series of differential conductance  $dI/dV$  spectra across one vortex. As expected,  $Z(\vec{r})$  is elevated within the vortex core, reflecting the suppression of superconductivity there. Figure 4(c) plots the vortex-induced  $Z(\vec{r})$  as a function of the radial distance from the vortex centers. An exponential decay of  $Z(r) = Z_\infty + A\exp(-r/\xi)$  fits the data well, resulting in a superconducting coherence length of  $\xi = 2.8 \pm 0.5$  nm.

Now we shed some light on the vortex pinning in  $\text{Sr}_{0.75}\text{K}_{0.25}\text{Fe}_2\text{As}_2$ . Charge doping has recently been argued to lead to collective pinning of vortices in Fe-SCs [26]. However, this charge model alone cannot account for the contrast between our observed vortex pinning in  $\text{Sr}_{0.75}\text{K}_{0.25}\text{Fe}_2\text{As}_2$  and the ordered vortices



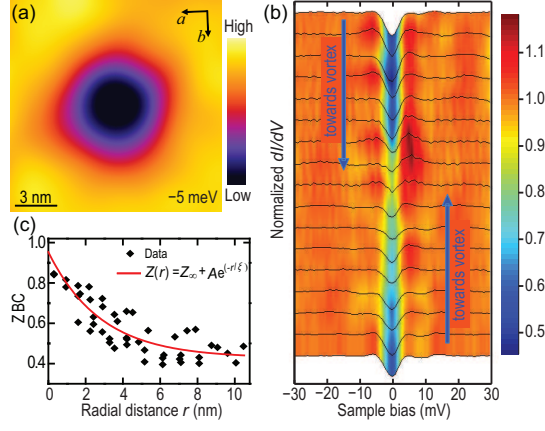


FIG. 4. (color online) (a) Average  $dI/dV$  at -5 meV from overlaying 48 single vortices. (b) Typical series of normalized  $dI/dV$  spectra straddling a single vortex. The spectra are equally separated and span a total distance of 11 nm. (c) Radial dependence of  $Z(r)$  around three vortices.

in  $\text{Ba}_{0.6}\text{K}_{0.4}\text{Fe}_2\text{As}_2$  with identical K dopants. Another possibility is that the shear modulus  $C_{66}$ , roughly proportional to  $H_{c2}b(1-b)^2$  (where  $b = H/H_{c2}$ ) [27], may play a role in the different vortex arrangements between  $\text{Ba}_{0.6}\text{K}_{0.4}\text{Fe}_2\text{As}_2$  and  $\text{Sr}_{0.75}\text{K}_{0.25}\text{Fe}_2\text{As}_2$ . A larger  $C_{66}$  often results in an ordered vortex lattice. Using the Ginzburg-Landau expression  $H_{c2} = \Phi_0/2\pi\xi^2$ , we estimate  $H_{c2} = 42 \pm 15$  T in  $\text{Sr}_{0.75}\text{K}_{0.25}\text{Fe}_2\text{As}_2$ , whereas  $H_{c2} \sim 75$  T in  $\text{Ba}_{0.6}\text{K}_{0.4}\text{Fe}_2\text{As}_2$  [11]. The persistence of vortex lattice order in  $\text{Ba}_{0.6}\text{K}_{0.4}\text{Fe}_2\text{As}_2$  down to 4 T (where the smaller  $C_{66}$  is comparable to that of  $\text{Sr}_{0.75}\text{K}_{0.25}\text{Fe}_2\text{As}_2$  at 9 T) [11] suggests that  $C_{66}$  can not solely account for the short-range vortex order in  $\text{Sr}_{0.75}\text{K}_{0.25}\text{Fe}_2\text{As}_2$ . Finally, we consider the nanoscale electronic inhomogeneities caused by K clustering, as hypothesized earlier. Note that the gap correlation length of  $\sim 3$  nm is comparable to the size of a single vortex core ( $\xi \sim 2.8$  nm). This indicates that the observed electronic irregularities may pin vortices [28] and disorder the vortex lattice. Since the ion size mismatch between  $\text{K}^+$  and  $\text{Ba}^{2+}$  is five times smaller than that between  $\text{K}^+$  and  $\text{Sr}^{2+}$  (see Table I), one can expect  $\text{K}^+$  ions to be less clustered in  $\text{Ba}_{0.6}\text{K}_{0.4}\text{Fe}_2\text{As}_2$  than in  $\text{Sr}_{0.75}\text{K}_{0.25}\text{Fe}_2\text{As}_2$  [29]. This leads to greater homogeneity and weaker vortex pinning, consistent with the well-ordered vortex lattices in  $\text{Ba}_{0.6}\text{K}_{0.4}\text{Fe}_2\text{As}_2$  [11]. In contrast, the large ion size mismatch between  $\text{K}^+$  and  $\text{Sr}^{2+}$  could account for the greater electronic inhomogeneity and disordered vortex lattice in  $\text{Sr}_{0.75}\text{K}_{0.25}\text{Fe}_2\text{As}_2$  observed here.

To quantify the effect of the ion size mismatch, we compute the correlation length of the vortex lattice  $\zeta = 39$  nm in Fig. 3(b) and several other Fe-SCs for comparison in Table I [22]. The larger  $\zeta = 128$  nm in

TABLE I. Ion size and vortex arrangement for several Fe-SCs.

Fe-SC	Native atom size (pm)	Dopant size (pm)	Diff. (pm)	$\zeta$ (nm)	Ref.
$\text{BaFe}_{1.8}\text{Co}_{0.2}\text{As}_2$	78	61	17	$22 \pm 1$	[5]
$\text{Sr}_{0.75}\text{K}_{0.25}\text{Fe}_2\text{As}_2$	126	146	20	$39 \pm 2$	
$\text{Ba}_{0.6}\text{K}_{0.4}\text{Fe}_2\text{As}_2$	142	146	4	$128 \pm 4$	[11]
FeSe	198	n/a	0	ordered	[20]
$\text{FeSe}_{0.4}\text{Te}_{0.6}$	198	221	23	disordered	[31]

$\text{Ba}_{0.6}\text{K}_{0.4}\text{Fe}_2\text{As}_2$  [11] can be explained by the smaller ion size mismatch, whereas the small  $\zeta = 22$  nm in  $\text{BaFe}_{1.8}\text{Co}_{0.2}\text{As}_2$  [5] can be explained by the large ion size mismatch there. Compared to  $\text{Sr}_{0.75}\text{K}_{0.25}\text{Fe}_2\text{As}_2$  which has a slightly larger ion size mismatch, the smaller  $\zeta$  in  $\text{BaFe}_{1.8}\text{Co}_{0.2}\text{As}_2$  suggests that  $\text{Co}^{3+}$  themselves, doped directly in the superconducting FeAs layer, may act as stronger pinning sites. Our hypothesis about the importance of dopant size mismatch is further supported in the  $\text{FeSe}_x\text{Te}_{1-x}$  system, where there is a large size mismatch between  $\text{Se}^{2-}$  and  $\text{Te}^{2-}$ . Although a homogeneous superconducting gap and ordered vortex lattice have been demonstrated in stoichiometric FeSe [20], both nanoscale chemical phase separation [30] and a disordered vortex arrangement [31] are seen in  $\text{FeSe}_x\text{Te}_{1-x}$ .

Finally we comment on the absence of quasiparticle bound states within the vortex cores [Fig. 4(b)] [32], which often appear as a pronounced peak at or near  $E_F$  in other Fe-SCs [11, 20, 23]. Using the residual resistivity  $\rho_0 = 0.08$  m $\Omega \cdot$  cm and Hall coefficient  $R_H = 1.16 \times 10^{-9}$  m $^3/\text{C}$  [13, 18], we obtain the electronic mean free path  $\ell = \hbar(3\pi^2)^{1/3}/e^2n^{2/3}\rho_0 \sim 5.2$  nm, two times bigger than  $\xi \sim 2.8$  nm. This suggests that our sample is macroscopically in the clean limit, where the vortex core bound states should have been observed. However, the vortices may be pinned in the relatively disordered regions, where the local mean free path is smaller [26]. Moreover, we note that the visibility of vortex core bound states apparently depends on the surface structure within the same material  $\text{Ba}_{0.6}\text{K}_{0.4}\text{Fe}_2\text{As}_2$  [11, 33].

In summary, our detailed STM/STS study of surface structure, superconducting gap, and vortex arrangement in  $\text{Sr}_{0.75}\text{K}_{0.25}\text{Fe}_2\text{As}_2$  has addressed four important questions on Fe-SCs. First, we have shown images and spectroscopy of the first large patches of unreconstructed  $1 \times 1$  surface on any  $\text{AFe}_2\text{As}_2$  material. This observation provides the final unambiguous evidence that both  $1 \times 2$  and  $\sqrt{2} \times \sqrt{2}$  reconstructions seen before represent a partial Sr layer. We observe no superconducting gap on the  $1 \times 1$  As surfaces, in contrast to the ubiquitous gap on  $1 \times 2$  surfaces, which reiterates the importance of attention to surface details when using STM/STS to study bulk superconductors. Second, we have explicitly shown by spatially resolved spectroscopy

that the gap varies on a 3 nm length scale, quite different from the 0.8 nm average distance between individual K dopants. This supports a local K clustering model. Third, we have imaged a vitreous vortex phase with a short-range hexagonal order ( $\zeta \sim 39$  nm), suggesting intermediate pinning strength between  $\text{BaFe}_{1.8}\text{Co}_{0.2}\text{As}_2$  and  $\text{Ba}_{0.6}\text{K}_{0.4}\text{Fe}_2\text{As}_2$ . Our hypothesis of the importance of dopant size mismatch provides a new avenue to optimize vortex pinning for increased critical current  $J_c$ . Fourth, we demonstrate an isotropic vortex structure and superconducting coherence length,  $\xi \sim 2.8$  nm. This constrains the pairing symmetry in  $\text{Sr}_{0.75}\text{K}_{0.25}\text{Fe}_2\text{As}_2$ , and helps to understand the nature of the superconducting mechanism in Fe-SCs.

We thank D. Inosov for helpful conversations. This work was supported by the Air Force Office of Scientific Research under grant FA9550-05-1-0371, and the U.S. National Science Foundation under grant DMR-0508812. C. L. S was supported by the Golub Fellowship at Harvard University.

---

\* jhoffman@physics.harvard.edu

- [1] Y. Kamihara, T. Watanabe, M. Hirano, and H. Hosono, *J. Am. Chem. Soc.* **130**, 3296 (2008).
- [2] I. I. Mazin, *Nature* **464**, 183 (2010).
- [3] J. T. Park *et al.*, *Phys. Rev. Lett.* **102**, 117006 (2009).
- [4] F. Massee, S. de Jong, Y. Huang, J. Kaas, E. van Heumen, J. B. Goedkoop, and M. S. Golden, *Phys. Rev. B* **80**, 140507 (2009).
- [5] Y. Yin, M. Zech, T. L. Williams, X. F. Wang, G. Wu, X. H. Chen, and J. E. Hoffman, *Phys. Rev. Lett.* **102**, 097002 (2009).
- [6] M. H. Julien, H. Mayaffre, M. Horvatić, C. Berthier, X. D. Zhang, W. Wu, G. F. Chen, N. L. Wang, and J. L. Luo, *Europhys. Lett.* **87**, 37001 (2009).
- [7] F. Massee, Y. Huang, R. Huisman, S. de Jong, J. B. Goedkoop, and M. S. Golden, *Phys. Rev. B* **79**, 220517 (2009).
- [8] M. Tropeano *et al.*, *Phys. Rev. B* **81**, 184504 (2010).
- [9] C. J. Van Der Beek, S. Demirdis, M. Konczykowski, Y. Fasano, N. R. Cejas Bolecek, H. Pastoriza, D. Colson, and F. Rullier-Albenque, *Phys. B: Condens. Matter* **407**, 1746 (2012).
- [10] J. E. Hoffman, *Rep. Prog. Phys.* **74**, 124513 (2011).
- [11] L. Shan *et al.*, *Nat. Phys.* **7**, 325 (2011).
- [12] M. Gao, F. J. Ma, Z. Y. Lu, and T. Xiang, *Phys. Rev. B* **81**, 193409 (2010).
- [13] G. F. Chen, Z. Li, J. Dong, G. Li, W. Z. Hu, X. D. Zhang, X. H. Song, P. Zheng, N. L. Wang, and J. L. Luo, *Phys. Rev. B* **78**, 224512 (2008).
- [14] F. C. Niestemski, V. B. Nascimento, B. Hu, W. Plummer, J. Gillett, S. Sebastian, Z. Q. Wang, and V. Madhavan, *arXiv:0906.2761* (2009).
- [15] M. C. Boyer, K. Chatterjee, W. D. Wise, G. F. Chen, J. L. Luo, N. L. Wang, and E. W. Hudson, *arXiv:0806.4400* (2008).
- [16] W. K. Yeoh *et al.*, *Phys. Rev. Lett.* **106**, 247002 (2011).
- [17] R. D. Shannon, *Acta. Cryst.* **32**, 751 (1976).
- [18] G. F. Chen, Z. Li, G. Li, W. Z. Hu, J. Dong, J. Zhao, X. D. Zhang, P. Zheng, N. L. Wang, and J. L. Luo, *Chin. Phys. Lett.* **25**, 3403 (2008).
- [19] P. Cai, X. D. Zhou, W. Ruan, A. F. Wang, X. H. Chen, D. H. Lee, and Y. Y. Wang, *arXiv:1208.3842* (2012).
- [20] C. L. Song *et al.*, *Science* **332**, 1410 (2011).
- [21] J. E. Hoffman, E. W. Hudson, K. M. Lang, V. Madhavan, H. Eisaki, S. Uchida, and J. C. Davis, *Science* **295**, 466 (2002).
- [22] D. S. Inosov *et al.*, *Phys. Rev. B* **81**, 014513 (2010).
- [23] T. Hanaguri, K. Kitagawa, K. Matsubayashi, Y. Mazaki, Y. Uwatoko, and H. Takagi, *Phys. Rev. B* **85**, 214505 (2012).
- [24] J. P. Reid *et al.*, *Phys. Rev. Lett.* **109**, 087001 (2012).
- [25] S. H. Pan, E. W. Hudson, A. K. Gupta, K. W. Ng, H. Eisaki, S. Uchida, and J. C. Davis, *Phys. Rev. Lett.* **85**, 1536 (2000).
- [26] C. J. van der Beek, M. Konczykowski, S. Kasahara, T. Terashima, R. Okazaki, T. Shibauchi, and Y. Matsuda, *Phys. Rev. Lett.* **105**, 267002 (2010).
- [27] E. H. Brandt, *Phys. Rev. B* **34**, 6514 (1986).
- [28] M. R. Eskildsen, E. M. Forgan, and H. Kawano-Furukawa, *Rep. Prog. Phys.* **74**, 124504 (2011).
- [29] P. Zajdel *et al.*, *J. Am. Chem. Soc.* **132**, 13000 (2010).
- [30] X. B. He, G. R. Li, J. D. Zhang, A. B. Karki, R. Y. Jin, B. C. Sales, A. S. Sefat, M. A. McGuire, D. Mandrus, and E. W. Plummer, *Phys. Rev. B* **83**, 220502 (2011).
- [31] T. Hanaguri, S. Niitaka, K. Kuroki, and H. Takagi, *Science* **328**, 474 (2010).
- [32] C. Caroli, P. G. De Gennes, and J. Matricon, *Phys. Lett.* **9**, 307 (1964).
- [33] Z. Y. Wang, H. Yang, D. L. Fang, B. Shen, Q. H. Wang, L. Shan, C. L. Zhang, P. C. Dai, and H. H. Wen, *Nat. Phys.* doi:10.1038/nphys2478 (2012).